Chinese Journal of
POLYMER SCIENCE

RESEARCH ARTICLE

https://doi.org/10.1007/s10118-026-3776-5
Chinese J. Polym. Sci.

Surface Morphologies and Dynamic Properties of Polyelectrolyte Brushes Induced by Charge Fraction and Cationic Size

Hong-Yan Zhang, Qing-Hai Hao*, Ming-Lu Chao, and Hong-Ge Tan*

College of Science, Civil Aviation University of China, Tianjin 300300, China

Abstract Understanding how the charge sequence along polyelectrolyte (PE) chains and the size of multivalent salt ions cooperatively regulates the behavior of polymer brushes is essential for the rational design of smart surfaces; however, a systematic mechanistic picture of their interplay remains elusive. In this study, we employed molecular dynamics simulations to systematically investigate the roles of the chain charge fraction and trivalent ion size in controlling the structural and dynamic properties of PE brushes. A series of intriguing brush-phase structures emerge from the interplay of these two parameters. Depending on the ion size range, the brush height exhibited three distinct responses to variations in charge fraction. Within different charge-fraction regimes, the brush height displays two contrasting responses to changes in ion size, namely monotonic and non-monotonic behavior. In the multi-chain regime, the structure factor increases monotonically with the charge fraction, whereas it shows a nonmonotonic dependence on the salt ion size. The block effect induced by the chain charge fraction and size effect of multivalent ions jointly give rise to a pronounced diversity in single-chain conformations. Furthermore, the diffusion coefficient revealed two distinct types of responses to the salt ion size, depending on the range of the charge fraction. These findings demonstrate that the synergistic interplay between the charge fraction and the trivalent cation size offers a versatile and powerful strategy for tailoring the equilibrium structures and chain dynamics of PE brushes, thereby providing valuable design guidelines for advanced responsive coatings.

Keywords Molecular dynamics simulations; Polyelectrolyte brushes; Charge fraction; Trivalent cation size; Coupled effects

Citation: Zhang, H. Y.; Hao, Q. H.; Chao, M. L.; Tan, H. G. Surface morphologies and dynamic properties of polyelectrolyte brushes induced by charge fraction and cationic size. *Chinese J. Polym. Sci.* https://doi.org/10.1007/s10118-026-3776-5

INTRODUCTION

Polyelectrolyte brushes (PEBs) have been widely used in diverse fields, such as drug delivery,[1] smart adhesion,[2–4] energy harvesting,[5] lubrication,[6–9] and biomedicine,[10] owing to their excellent responsiveness to external stimuli and wide applications. The behavior of PEBs depends on both the brush design and physical environment.[11] Previous studies have demonstrated that the charge fraction of the PEB, pH of the surrounding medium, and ion size and valence each induce significant effects on the brush.[12–18] For example, the charge fraction of the brush[17] and parameters such as the size[16] and valence of salt ions[14,18] directly influence the extension state of PEB and the stability of the brush layer.

To further optimize the design and expand the applications of PEBs, extensive research has been conducted on how the charge fraction influences the structure of the PEBs, thereby affecting their interfacial function. Gioldasis *et al*.[19] studied the effects of charge fraction on the height of zipper brushes and their internal structure using molecular dynamics (MD) simulations. They found that the charge fraction of anionic PEB significantly influenced the internal structure of the zipper brushes formed by PEB and cationic-neutral diblock copolymers. When the charge fraction of the PEB was 0.2, the zipper brushes formed a perforated film at a moderate grafting density. When the charge fraction was 0.4, the zipper brushes adopted a pinned micellar structure. Further increasing the charge fraction of the PEB to 1.0 resulted in a reversed U-tube structure. Using all-atom MD simulations, Das *et al*.[12] studied the effect of the charge fraction on PE brushes. They found that with increasing charge fraction, inter-chain repulsion increased and brush height increased slightly until saturation at a high grafting density. Using coarse-grained MD simulations and self-consistent field theory (SCFT), Smook and de Beer[17,20] systematically studied the effect of charge fraction on the electroresponse of PE brushes. Specifically, the PE brushes displayed an optimal electroresponse when the charge fraction ranged from 14% to 22%.

In recent years, there has also been growing interest in clarifying the ion size and ion valence-induced collapse of PE brushes. Prusty *et al*.[21] found that for PE brushes with alternating charges, the brush height was insensitive to the anion size at low salt concentrations, whereas at high salt concentrations, it decreased as the anion size increased. Moreover, the total brush height of the diblock PE brushes was more sensitive to ion size variations than that of the alternating PE

* Corresponding authors, E-mail: qhhao@cauc.edu.cn (Q.H.H.)
E-mail: hgtan@cauc.edu.cn (H.G.T.)
Received May 8, 2026; Accepted June 9, 2026; Published online September 20, 2026

brushes under high salt concentrations. Duan *et al*.[22] investigated the behavior of PE brushes in multivalent salt solutions using SCFT. They found that reducing the radius of the multivalent cation significantly enhanced ion correlations, leading to the formation of an oscillatory layer structure in PE brushes at high grafting densities. Using a surface force apparatus (SFA) and atomic force microscopy (AFM), Yu and coworkers[16,18,23,24] observed that multivalent ions were more effective than monovalent ions in reducing the height of the PE brushes. They also reported that for divalent ions, differences in ionic size resulted in distinct effects on both the structure and height of the PE brushes. On the basis of all-atom MD simulations, the Das' team[15] found that the degree of binding of counterion on the PE brushes decreased in the order I^- > Br^- > Cl^- > F^-, consequently leading to the smallest brush height with I^- ions and the largest height with F^- ions. Through coarse-grained MD simulations, Jackson *et al*.[25] discovered that multivalent ions induced heterogeneous collapse of PE brushes in good solvents by bridging effects, whereas monovalent ions exhibited a relatively weak effect on brush height and no obvious lateral heterogeneous structure was observed. Kim *et al*.[26] experimentally investigated the effect of the gold nanoparticle size on electrostatic adsorption onto PE brushes. They found that both large and small AuNPs coexisted on the PE brush surface under salt-free conditions. However, as the salt concentration increased, the adsorption of small gold nanoparticles onto the PE brushes rapidly weakened, whereas larger gold nanoparticles remained selectively adsorbed.

Although extensive research has revealed the distinct effects of charge fraction or ion specificity on the PE brush structure, a systematic understanding of their coupled effects is still lacking. To date, several studies have made progress in understanding the behavior of PE under the coupling of charge fraction and ion specificity. Philippova *et al*.[27] reported a combined experimental and theoretical study, and the results showed that the charge fraction and ion size cooperatively influenced the swelling behavior of PE gels. Large ions induced continuous swelling of the gel with increasing charge fraction, whereas small ions resulted in initial swelling, followed by collapse and eventual stability. In contrast, intermediate ions induced a three-stage response in the PE gels, characterized by initial swelling, subsequent collapse, and final reswelling with a charge fraction. Recently, Tagliabue and Mella[28] systematically investigated the influence of charge density and counterion size on the conformation of star-shaped polyelectrolytes and ion behavior using Langevin dynamics simulations. They found that the rigidity of the chain was enhanced by either the size of the ions or the charge density of the PE brushes. Through coarse-grained MD simulations, in this study, we focus on planar PE brushes and investigate the effects of salt cation size on their surface morphology and dynamic properties under different charge fractions to obtain the optimal values of charge fraction and ion size for stimuli-responsive PE brushes.

MODEL AND SIMULATION DETAILS

In our simulations, a coarse-grained bead-spring model composed of individual PE chains was used for the planar grafted PE brush. Each PE chain contained N=60 monomers connected by covalent bonds. It consists of two types: neutral and charged monomers. Each charged monomer carries one unit of negative charge -e. The charged monomers were placed next to each other within every ten monomers. The charge fraction f was set from 0.1 to 1.0. For f=0.1, every ten monomers carry one negative charge. For f=0.3, within every ten monomers, three are charged, and these three charged monomers are next to each other, as illustrated in Fig. 1.

PE chains were anchored by one end to a planar substrate in a 10 × 10 square array with a fixed chain number of M=00. The grafting density, σ_g is fixed at 0.01. The size $L_x \times L_y \times L_z$ of the simulation box was $100\sigma \times 100\sigma \times 300\sigma$. The planar substrate was located at z=0, and a non-selective, impenetrable neutral wall was placed at $z = L_z = 300\sigma$ to prevent the escape of mobile particles. Periodic boundaries were applied in the x and y directions. Trivalent cations, monovalent anions, and counterions were randomly added to the simulation box. The number of trivalent salt cations is equal to one-third that of the charged monomers, as this corresponding salt concentration is most conducive to analyzing the size specificity of the salt cations. Under this charge stoichiometry condition, the concentration of trivalent salt cations C_{S^+} is given by $C_{S^+} = NMf/(3L_xL_yL_z)$, and the salt ionic strength I is expressed as $I = \frac{1}{2}(C_{S^+}z_+^2 + C_{S^-}z_-^2) = \frac{2NMf}{L_xL_yL_z}$, where z_+ and z_- are the valences of salt cations and anions, C_{S^-} is the concentration of monovalent salt anions. Thus, the salt ionic strength scales linearly with the charge fraction f in the simulations.

The interaction between any two particles in the system is described by the standard shifted and truncated Lennard-

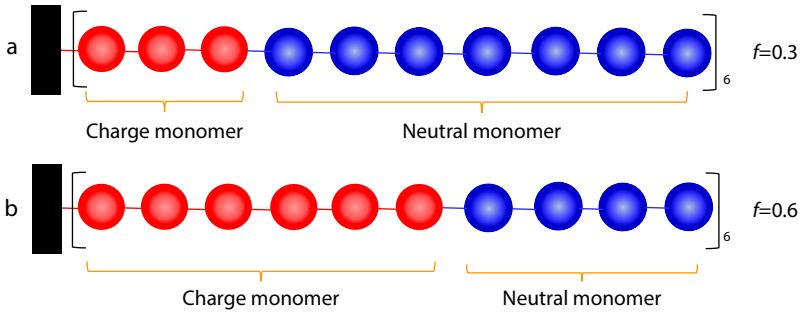

Fig. 1 Schematic representation of PE chains at (a) f=0.3 and (b) f=0.6.

https://doi.org/10.1007/s10118-026-3776-5

Jones (LJ) potential:

$$U_{\mathrm{LJ}}(r_{ij}) = \begin{cases} 4\varepsilon_{\mathrm{LJ}}\left[\left(\frac{\sigma_{ij}}{r_{ij}}\right)^{12} - \left(\frac{\sigma_{ij}}{r_{ij}}\right)^{6} - \left(\frac{\sigma_{ij}}{r_{\mathrm{c}}}\right)^{12} + \left(\frac{\sigma_{ij}}{r_{\mathrm{c}}}\right)^{6}\right] & r_{ij} \le r_{\mathrm{c}} \\ 0 & r_{ij} > r_{\mathrm{c}} \end{cases} \quad (1)$$

where r_{ij} is the distance between the i^{th} and j^{th} particles, $\varepsilon_{\mathrm{LJ}} = 1.0k_{\mathrm{B}}T$ is the interaction strength of the LJ potential. where k_{B} is the Boltzmann constant, and T is the absolute temperature. Parameter σ_{ij} is defined as $(\sigma_i + \sigma_j)/2$, where σ_i and σ_j denote the diameters of the i^{th} and j^{th} particles, respectively. A cutoff radius $r_{\mathrm{c}} = 2^{1/6}\sigma_{ij}$ corresponds to good solvent conditions for the polymer backbone. In our simulation, the diameter of the salt cations varies from 0.1 to 3.0, whereas the diameters of the other particles were uniformly set to 1.0, with a length scale defined as σ.

The neighboring monomer particles along the chain are connected by a finite extension nonlinear elastic (FENE)[29,30] potential:

$$U_{\mathrm{FENE}}(r_{ij}) = -\frac{1}{2}KR_{\max}^2 \ln\left[1 - \left(\frac{r_{ij}}{R_{\max}}\right)^2\right] \quad (2)$$

where $K = 30.0k_{\mathrm{B}}T/\sigma$ is the bond strength, and $R_{\max} = 1.5\sigma$ is the maximum bond length.

The electrostatic interaction between any two charged particles q_i and q_j, is modeled by the Coulomb potential energy:

$$U_{\mathrm{Coul}}(r_{ij}) = k_{\mathrm{B}}T\frac{\lambda_{\mathrm{B}}q_iq_j}{r_{ij}} \quad (3)$$

where λ_{B} is the Bjerrum length, which was set to 3.0σ in the simulations. The particle-particle particle-mesh (PPPM) algorithm was used to calculate the Coulomb potential with an estimated accuracy of 10^{-3}.

MD simulations were performed in a canonical ensemble using the open-source software, LAMMPS.[31] The motion of any particle is described by the Langevin equation:

$$m\frac{\mathrm{d}^2\mathbf{r}_i(t)}{\mathrm{d}t^2} = -\nabla U_i - \xi\frac{\mathrm{d}\mathbf{r}_i(t)}{\mathrm{d}t} + \mathbf{F}_i^R(t) \quad (4)$$

where m=1.0 is the uniform particle mass for all types, and $\mathbf{r}_i$ is the position vector for each particle. U_i denotes the total potential of the system and ξ is the friction coefficient. $\mathbf{F}_i^R(t)$ is the stochastic force with an average value of zero that satisfies the fluctuation dissipation theorem. All the physical quantities were unified using an LJ unit system. The friction coefficient was ξ = 0.143 $m\tau^{-1}$,[32,33] where $\tau = \sigma(m/\varepsilon_{\mathrm{LJ}})^{1/2}$ is the standard LJ time unit. The equation of motion was solved using the velocity-Verlet algorithm with a time step of $\Delta t = 0.005\tau$.

The system was first heated to T=3.0 for 2×10^6 time steps to remove dependence on the initial configuration. The system was then gradually cooled down to T=1.0, over 4×10^6 time steps, followed by 6×10^6 time steps for equilibration. Finally, a production run with 8×10^6 time steps was performed. During the production run, the simulation saved a snapshot every 2×10^3 time steps. In addition, all simulation processes were independently performed thrice to ensure statistical consistency. Because the three replicates produced similar results, only one representative replica is presented.

RESULTS AND DISCUSSION

Autocorrelation Function

To ensure the validity of the simulation results, we must evaluate whether the system has reached a steady state. In our simulations, we calculate the autocorrelation function $C_{\mathrm{H}}(t)$ of the brush height to monitor the system equilibrium, which is defined as

$$C_{\mathrm{H}}(t) = \frac{\langle\delta H(t)\delta H(0)\rangle}{\langle H^2\rangle - \langle H\rangle^2}, \delta H(t) = H(t) - \langle H\rangle \quad (5)$$

where H is the PE brush height and can be calculated by:

$$H = \frac{2\int_0^{L_z} z\rho_{\mathrm{M}}(z)\mathrm{d}z}{\int_0^{L_z}\rho_{\mathrm{M}}(z)\mathrm{d}z} \quad (6)$$

where L_z denotes the height of the simulation box in the z-direction and $\rho_{\mathrm{M}}(z)$ is the vertical density distribution of the monomers as a function of the distance from the substrate.

Fig. 2 plots the autocorrelation function $C_{\mathrm{H}}(t)$ of the brush height for different salt-cation diameters. It is observed that, under all conditions of salt cation size, $C_{\mathrm{H}}(t)$ starts oscillating near 700τ and, after this time point, decays almost to a stable pattern, indicating that the system has reached stability. This time point is much shorter than the total simulation duration of $4\times10^4\tau$ in this study. Therefore, it can be confirmed that the

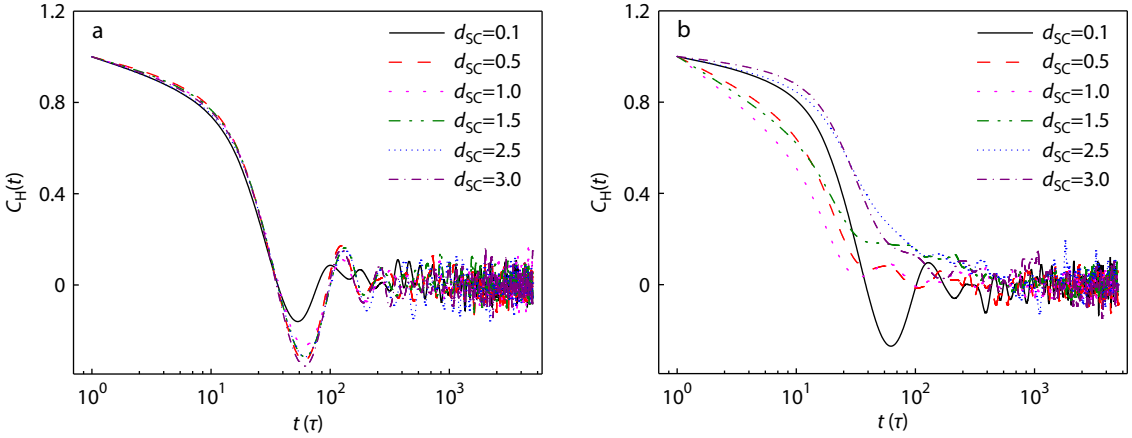

Fig. 2 Autocorrelation function $C_{\mathrm{H}}(t)$ of the brush height with (a) f=0.1 and (b) f=1.0 for different salt cation diameters.

system has reached a steady state well within the simulation time, and thus our simulation results are reliable.

It is important to clarify that, in this study, $C_H(t)$ was calculated for systems with charge fractions from f=0.1 to 1.0, and salt cation sizes ranging from d_{SC}=0.1 to 1.0, aiming to verify whether the systems had reached equilibrium. $C_H(t)$ for all systems oscillated near zero until the end of the full simulation, indicating that equilibrium was achieved. For clarity, we present only the autocorrelation results for the representative charge fractions f=0.1 and f=1.0.

Surface Morphologies

The simulation snapshot provides an intuitive visualization of the surface morphological evolution of the PE brushes. To more effectively demonstrate the effect of the salt cation size on the PE brushes with varying charge fractions, we generated snapshots of the PE brushes based on simulation data, as depicted in Fig. 3.

Fig. 3 illustrates the dependence of the surface morphology on the charge fraction, which varied significantly with the size of the salt cation. When the salt cation was small d_{SC}≤0.3 (the first two lines in Fig. 3), the PE brushes remained homogeneous regardless of the charge fraction. Even with a substantial increase in the charge fraction, only the curling tendency of the individual chains was observed. The reason for this behavior is that at low charge fractions, the large spacing between the charged monomers along the PE chains prevents the small multivalent cations from affecting intra-chain bridging, permitting the chains to extend under good solvent conditions. As the charge fraction increases, the reduced distance between neighboring charged monomers enables intrachain bridging to induce gradual chain coiling. However, owing to the small cation size, the inter-chain effects remain negligible, leading to a homogeneous collapsed structure composed of individually coiled chains.

For moderate salt cation sizes (0.5≤d_{SC}≤1.5), increasing the charge fraction drives the transition of the brushes from a homogeneous state to a laterally heterogeneous morphology. This structure is comprised of multiple substrate-anchored PE chains that assemble into pinned micelles. The formation of these micelles is attributed to the enhanced inter-chain bridging mediated by moderate-sized cations at higher charge fractions.

For relatively large cations (d_{SC}≥2.0), the electrostatic attraction between the cations and monomers is weakened, and the excluded volume effect of the cations becomes significant. By contrast, larger cations provide a larger contact surface area, which directly facilitates the cation-mediated inter-chain bridging effect. These effects are further enhanced at high charge fractions because of the increased amounts of charged monomers and cations. Under the interplay of these factors, the chains preferentially undergo large-scale lateral loose aggregation, rather than forming discrete pinned micelles. Upon increasing the salt cation diameter to d_{SC}=3.0, the system forms a homogeneous swollen layer structure.

Furthermore, at a fixed charge fraction, the brush morphology exhibited a clear dependence on cation size. Specifically, as the cation size increases, the brush structure evolves sequentially from homogeneous to laterally heterogeneous and

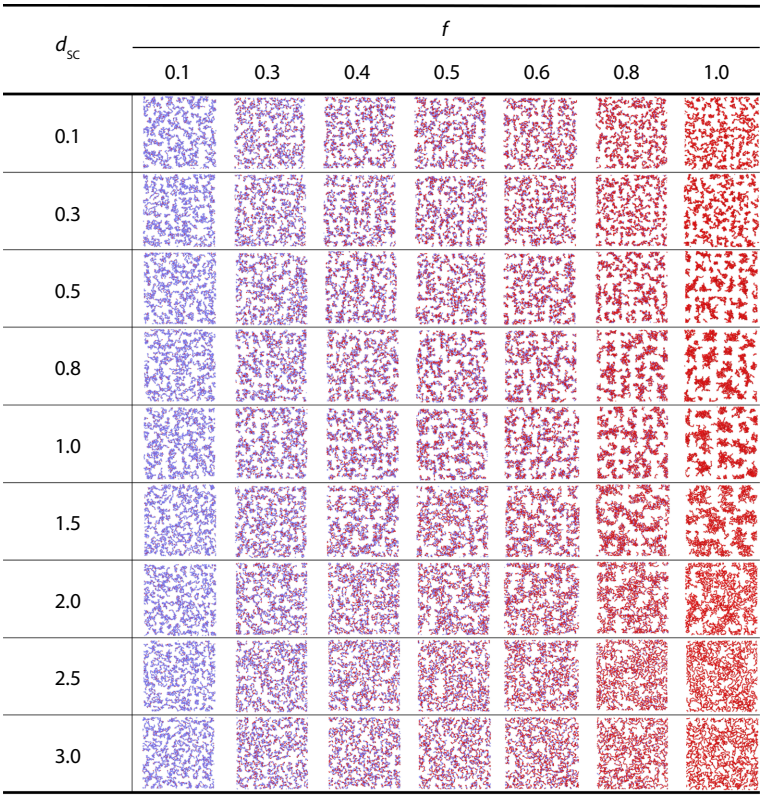

Fig. 3 Top view of planar PE brushes as the variation of charge fractions in the presence of different salt cation diameters. Red beads and transparent blue beads represent charged and neutral monomers respectively.

https://doi.org/10.1007/s10118-026-3776-5

finally to homogeneous layer structures. This trend was most pronounced at f=1.0, as shown in the right column of Fig. 3. Remarkably, this trend is directly corroborated by the experimental work of Xu *et al.*[16] In their study, Mg^{2+} and Ca^{2+} (the smaller cations) induced a uniformly collapsed structure of the PE brushes, whereas Ba^{2+} (the largest) led to pronounced lateral inhomogeneity. Given that the ionic radii follow Mg^{2+} < Ca^{2+} < Ba^{2+} and that all these cations are smaller than the PSS monomer size at f=1.0, the experimental observations are in excellent agreement with our simulated ion-specific morphology evolution at the full charge fraction. Beyond this validation, our simulations further explored the regime f<1.0. It was revealed that, governed by the interplay of electrostatic screening, inter-chain bridging, and steric effects, ion-specific responsiveness persists across partially charged brushes, albeit with modified thresholds and extent of lateral nonuniformity.

In-plane Static Structure Factor of Monomers

To quantify the long-range order of the lateral patterns of the PE brushes, we calculated the in-plane structure factor between charged monomers, defined as follows:

$$S_{xy}(k) = \frac{1}{N_m}\left\langle \sum_{i=1}^{N_m}\sum_{j=1}^{N_m} e^{-i\mathbf{k}\cdot(\mathbf{r}_i-\mathbf{r}_j)}\right\rangle - N_m\delta_{k,0} \quad (7)$$

where $\delta_{k,0}$ is the Kronecker delta function, N_m is the total number of charged monomers in the system, $\mathbf{r}_i$ and $\mathbf{r}_j$ are the in-plane position vectors of the i^{th} and j^{th} charged monomers, respectively, and $\mathbf{k}$ is the in-plane wave vector discretized based on the size of the simulation box. $S_{xy}(k)$ was calculated by first integrating over the wave vector space of $|\mathbf{k}| = k$ and then averaging over the trajectories. For clarity, only four representative charge fractions (f=0.1, 0.3, 0.6, and 1.0) based on the charge fraction dependence of the PE brushes are provided for each salt cation diameter.

As shown in Fig. 4, all profiles exhibited a peak at $\mathbf{k}$ = $0.65\sigma^{-1}$, indicating a periodic structure with a characteristic length scale of $L \approx 2\pi/k \approx 9.66\sigma$. This scale corresponds precisely to the inter-chain grafting distance, confirming that this peak arises from the single-chain area with a theoretical size of $1/\sigma_g$ = 10.0σ. Consequently, the peaks appearing at k < $0.65\sigma^{-1}$ (*i.e.*, $L \geq 9.66\,\sigma$) correspond to the multi-chain domains within the PE brushes.

The structure factor shows a clear dependence on the charge fraction f. With increasing f, the intensity of the multi-chain peaks increases relative to that of the single-chain peak, indicating that multi-chain structures become progressively more dominant. Specifically, for $f \leq 0.3$, as shown in Figs. 4(a) and 4(b), the multi-chain peak intensity was significantly lower than that of the single-chain peak, indicating that the brushes primarily adopted single-chain conformations. In contrast, at a high f demonstrated in Figs. 4(c) and 4(d), the

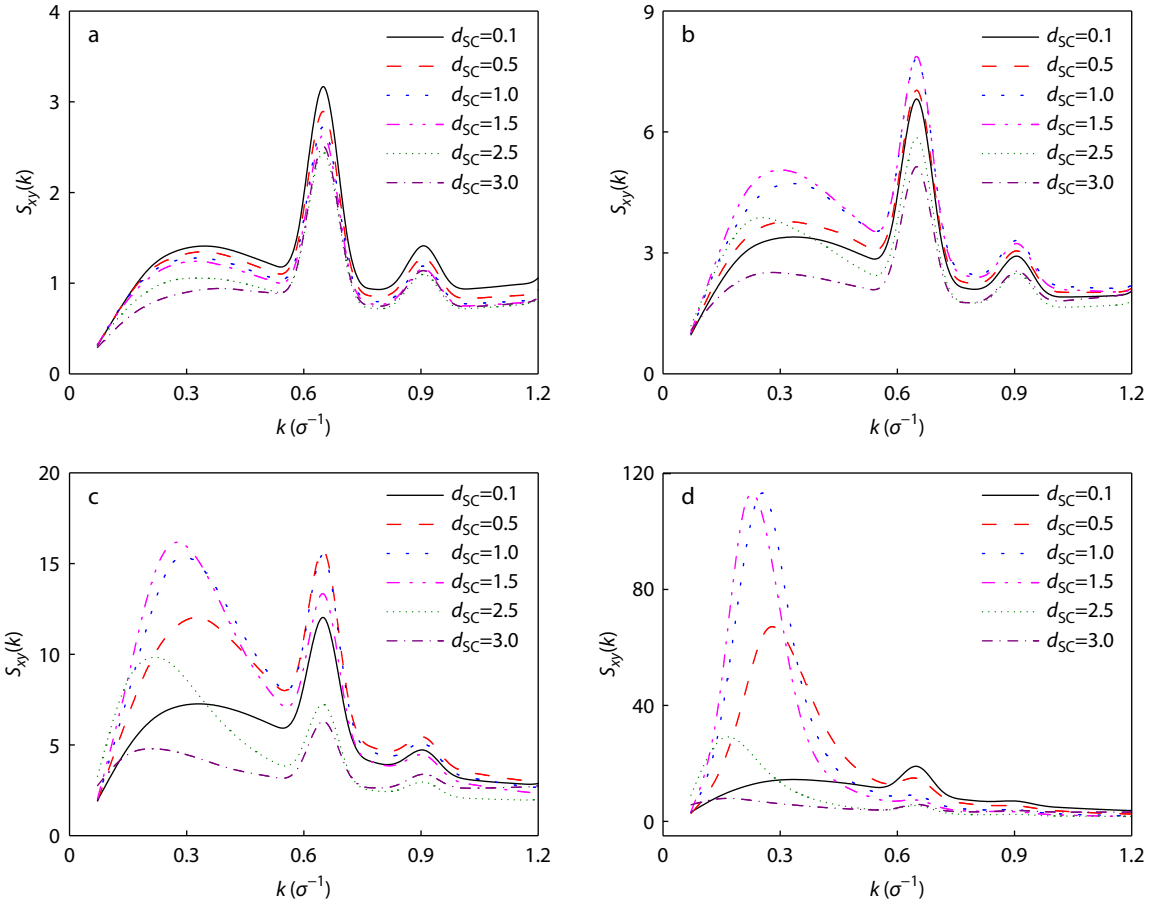

Fig. 4 In a two-dimensional plane static structure factors of charged monomers at varying cationic sizes for different chain charge fractions. (a) f=0.1, (b) f=0.3, (c) f=0.6, (d) f=1.0.

https://doi.org/10.1007/s10118-026-3776-5

multi-chain peak intensity substantially exceeds that of the single-chain feature, signifying that multi-chain aggregates dominate the surface microphase separation morphology.

Moreover, the structure factor also showed a distinct response to ion size. As shown in Fig. 4(a), at a low charge fraction f=0.1, the multi-chain peak intensity decreases slightly and monotonically with increasing cation size. However, for f≥0.3, the multi-chain peak intensity varies non-monotonically with the cation size, reaching a maximum at d_{SC}=0.8 and 1.0. This maximum suggests that the formation of distinct lateral pinned micelles induced by the inter-chain bridging of trivalent cations is optimal within this specific cation size range. While this non-monotonic trend resembles the brush height response in Fig. 5(b), a slight shift in the turning point is expected because the brush height probes the longitudinal structure, whereas the structure factor primarily reflects transverse correlations. Furthermore, when the multi-chain structure is notably prominent (Figs. 4c and 4d), the characteristic peak of the multi-chain structure shifts monotonically to lower k with increasing cation diameter, indicating an increase in the real-space dimensions of the multi-chain domains. This trend is consistent with the morphological evolution observed in the top-view images in Fig. 3.

Brush Height

The Brush height serves as a core structural parameter of PE brushes, reflecting fundamental characteristics such as chain length and grafting density. Here, we investigated the influence of the salt cation size and charge fraction in the PE chain on brush height, as shown in Fig. 5.

As shown in Fig. 5(a), the brush height exhibited three distinct profiles as a function of the charge fraction. For a small salt cation diameter (*e.g.*, d_{SC}=0.1, indicated by black solid squares), the brush height displays a weak oscillatory dependence on f, with local maxima at f=0.3, 0.6, and 0.9. This oscillation arises from the charge stoichiometry effect. At f=0.3, each charged block carries three negative charges that exactly neutralize one trivalent salt cation, promoting complete cation adsorption around the charged block. These blocks tended to wrap tightly around the cation, forming knot-like structures along the chain (Fig. 5c). Such knot-like configurations enhance chain rigidity,[34] leading to slight expansion of the brushes. Analogous stoichiometric matching at f=0.6 and 0.9, similarly facilitates knot formation, resulting in modest height increases at these charge fractions.

For moderate cation sizes (0.5≤d_{SC}≤1.5), the brush height decreases monotonically with increasing f. This behavior is attributed to the combined bridging effect of multivalent cations and screening effect (*i.e.*, the addition of multivalent cations screens the electrostatic repulsion between charged monomers). As the charge fraction increased, a higher concentration of trivalent cations more effectively screened the repulsion while simultaneously enhancing cation-mediated inter-chain bridging. Both effects promote chain aggregation, thus reducing brush height. For cation sizes d_{SC}>2.0, the brush height increases monotonically with f. Here, the excluded volume effect of bulky salt cations dominates, progressively swelling the brushes as the charge fraction increases.

Our simulation results align qualitatively with the experimental findings of Philippova and co-workers[27] on the swelling behavior of PE gels yet reveal important distinctions arising from the different geometric constraints. In their gel system, bulky tetrabutylammonium ions induced monotonic swelling upon ionization, which is consistent with our large-cation regime. For small counterions (Na^+ and Cs^+), the gels initially swelled but then collapsed as the ionization degree increased. With intermediate-sized ions (tetramethyl and tetraethylammonium), the gels exhibited a more complex response: swelling, followed by collapse, and finally reswelling.

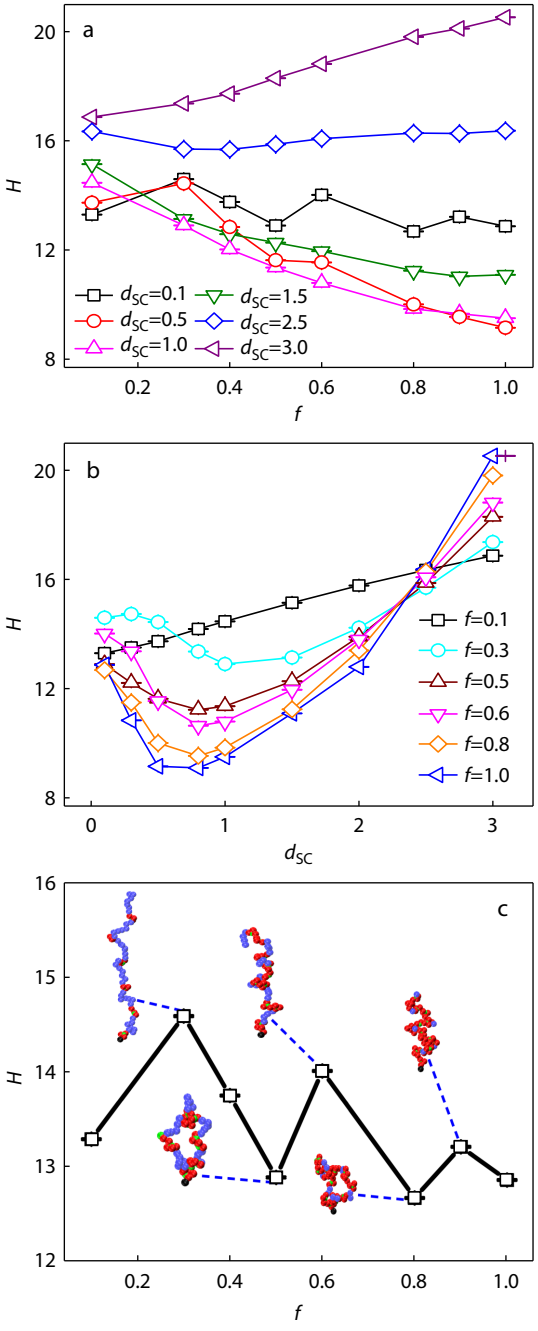

Fig. 5 (a) The brush height as a function of chain charge fraction at the varying salt-cation sizes; (b) The brush height as a function of salt-cation size at the varying chain charge fractions; (c) The typical chain conformation for d_{SC}=0.1 is illustrated.

https://doi.org/10.1007/s10118-026-3776-5

This contrasts with our brush system, where small cations produce only weak oscillatory height variations and intermediate cations yield a monotonic decrease in height. These discrepancies are rooted in the different spatial constraints of the two systems. Gels swell or collapse isotropically in three dimensions, allowing a wide range of conformational responses. In contrast, PE brushes are tethered at one end to a grafting surface, confining their degrees of freedom primarily to extend normally to the surface.

To further elucidate the effect of the cation size, we examined the dependence of the brush height on the salt cation diameter d_{SC}, as shown in Fig. 5(b). The brush height exhibits two distinct regimes with increasing cation size: a monotonic increase at a low charge fraction (f=0.1) and non-monotonic behavior at higher f.

Specifically, at f=0.1, the brush height increased monotonically with d_{SC}. This trend arises because of two factors. First, the adsorbed salt cations themselves become larger, which directly contributes to the increased brush height. Second, owing to the charge mismatch between the negatively charged monomers (each carrying $-e$) and the adsorbed trivalent cations (each carrying $+3e$), the grafted PE chains possess a net positive charge. The electrostatic repulsion between these net charges further expands the brushes, leading to an increase in the brush height.

At higher charge fractions, the brush height depends non-monotonically on d_{SC}. It initially decreased, reached a minimum, and then increased. This non-monotonicity becomes more pronounced as f increases and is characterized by a lower minimum and a higher maximum brush height. Notably, the minimum consistently occurred within the cation size range of d_{SC}=0.8–1.0, corresponding to the morphologies shown in Figs. 4(b)–4(d). This behavior can be explained by the competition among bridging, screening, and excluded volume effects. In the range of d_{SC}=0.1–1.0, increasing the cation size enhances both the bridging effect and electrostatic screening, which together promote the aggregation of charged monomers and thereby reduce brush height. The experimental and all-atom simulation observations supported this trend. Xu *et al*.[16] and Das *et al*.[15] have demonstrated that, at a fixed charge fraction, larger ionic radii (*e.g.*, Ba^{2+} > Ca^{2+} > Mg^{2+} among alkaline earth metals, or I^- > Br^- > Cl^- > F^- among halides) lead to a lower PE brush height. Similarly, Kim *et al*.[26] found that as the nanoparticle size increased, PE brushes preferentially adsorbed larger nanoparticles, resulting in a reduced brush height. These findings are consistent with our simulated results in the regime where the salt cation size is smaller than the monomer size (d_{SC}≤1.0).

Beyond this range (d_{SC}>1.0), the excluded volume effect of the bulky cations became dominant, leading to a subsequent increase in the brush height. This large-size regime behavior is corroborated by prior computational and experimental studies. Tagliabue and Mella[28] reported that in star-shaped PEs, the chains gradually expand with increasing counterion size in the large-size limit. Likewise, Philippova *et al*.[27] observed that under large-cation conditions, the radius of gyration of PE chains increases monotonically with cation size, indicating progressive chain extension. Both findings align well with our simulated results for the large d_{SC} regime.

Mean Bond Angles of the PE Chains

To further clarify the conformation of the PE chains, the average bond angle Φ_i between the neighboring bonds was calculated, and the results are shown in Figs. 6 and 7.

As shown in Fig. 6(a), at a charge fraction of f=0.1, the bond angles formed between adjacent bonds in the PE chains were obtained, indicating that the chains adopted a relatively extended conformation. This behavior is due to the fact that the chains are predominantly composed of neutral monomers at low charge fractions, and the intra-chain bridging effect induced by salt cations is not substantial, resulting in larger bond angles. Notably, distinct periodic peaks were observed, which were more pronounced for the small cations, primarily originating from the periodic arrangement of charged and neutral segments along the chain, combined with the electrostatic attraction between the charged monomers and salt cations. As the size of the salt cations increased, this periodicity became progressively less pronounced, suggesting that the charged segments themselves became more extended. This trend was mainly attributed to the increasing steric volume of the cations, as illustrated in the inset of Fig. 6(a). Furthermore, with increasing cation size, the overall decrease in $\langle \cos\Phi_i \rangle$ values reflects an increase in all bond angles, indicating that the single chain becomes increasingly extended as ion size grows. This observation is consistent with the trend in brush height shown in Fig. 5(b) at f=0.1.

As the charge fraction increased to f=0.3, as shown in Fig. 6(b), the curves exhibited periodic undulations with a period of 10 monomers regardless of the size of the salt cations. This periodicity reflects the alternating distribution pattern of the charged monomers along the chain. When the trivalent cations are small, the peaks in the curve align precisely with the central positions of the charged blocks, as illustrated in the inset of the first panel in Fig. 6(b). This behavior arises from the fact that each charged block interacts strongly with trivalent salt cations, and the electrostatic attraction between adjacent charged monomers leads to a reduction in bond angles within the charged segments. As d_{SC} increased, the peaks diminished rapidly and the original peak positions gradually transformed into troughs. This indicates a marked increase in bond angles at these sites, suggesting that the charged block segments transition from a bent to an extended conformation. This transition is also attributable to the steric volume effect of the salt cations. Furthermore, the degree of extension of the neutral segments was also modulated by the size of the salt cations, as indicated by the cosine values shown by the dashed line in Fig. 6(b). The bond angles of the neutral segments were observed to first decrease and then increase, with the transition occurring at d_{SC}=1.0, exhibiting a non-monotonic variation with the diameter of the cations similar to that of the brush height shown in Fig. 5(b).

As illustrated in Fig. 7, for a small salt cation (d_{SC}=0.1), the $\langle \cos\Phi_i \rangle$ profile exhibited a periodic multimodal pattern. At f=0.6 (Fig. 7a), the charge ratio between the charged segment and the salt cation is 2:1; accordingly, the profile displays a periodic bimodal pattern with peaks centered at the positions of the charged monomers (see the inset of the upper panel in Fig. 7a). When the charge fraction increases to

https://doi.org/10.1007/s10118-026-3776-5

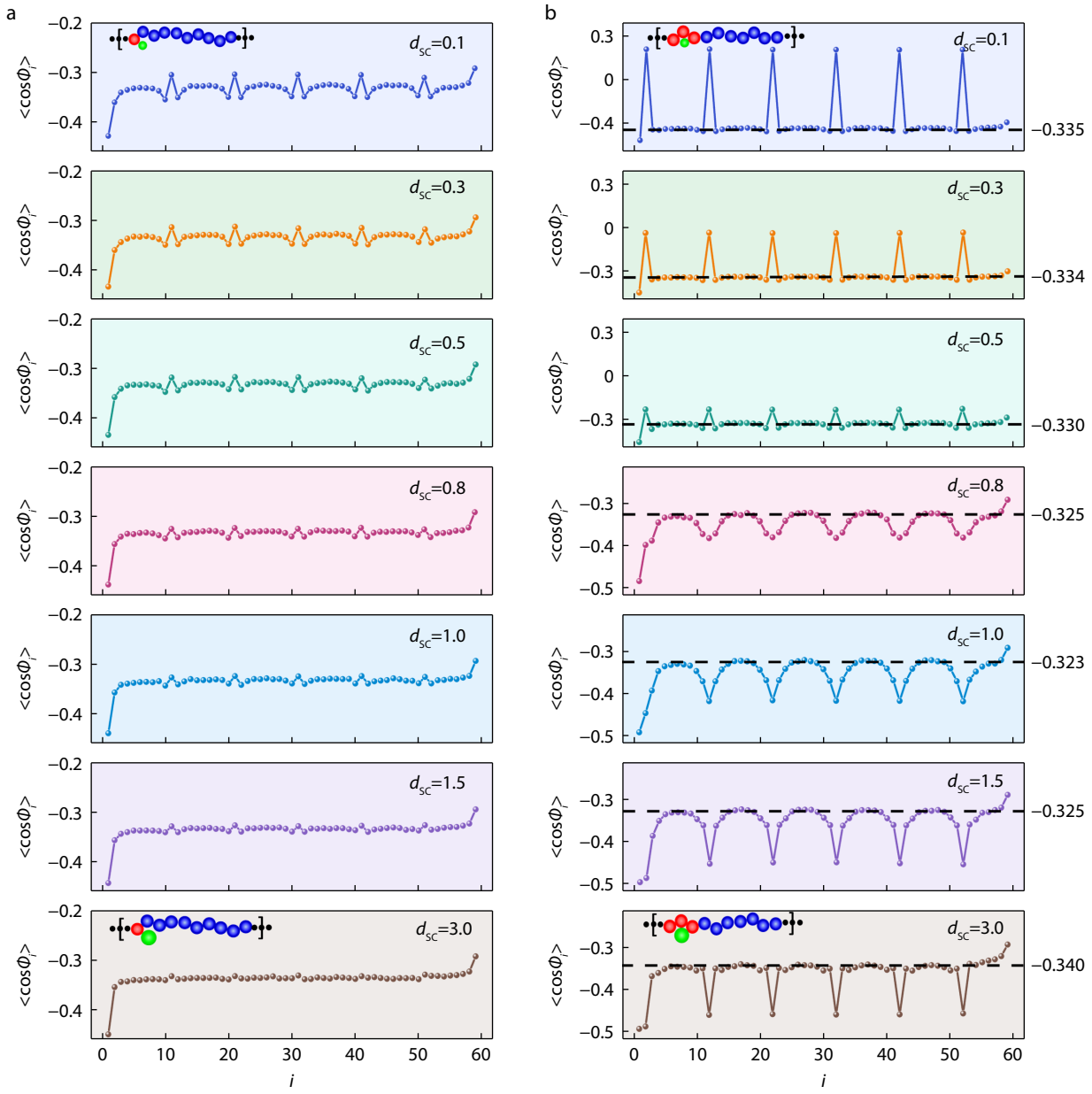

Fig. 6 $\langle\cos\Phi_i\rangle$ of adjacent monomer bond angles as a function of bond sequence i in a single chain, considering different chain charge fractions: (a) f=0.1 and (b) f=0.3. The inset shows the chain configuration under these conditions. The dashed lines in the right panels represent the cosine values of the bond angles between adjacent neutral monomers.

f=0.9 (Fig. 7b), the charge ratio between the segment and salt cation becomes 3:1. Consequently, the $\langle\cos\Phi_i\rangle$ curve presents a periodic triple-peak structure, analogous to that observed at f=0.6.

As the salt cation size increases to d_{SC}=0.5, The electrostatic bridging effect induced by multivalent cations begins to emerge as the salt cation size increases to d_{SC}=0.5. As a result, at f=0.6, the bimodal feature gradually transitions into a unimodal profile, whereas at the higher charge fraction of f=0.9, the triple-peak pattern gradually disappears. Upon further increasing the cation size, the steric volume effects become dominant. The peaks corresponding to the charged segments progressively diminish and eventually evolve into troughs. This transition indicates a substantial increase in the bond angles within the charged segments.

Mean Square Displacement

In this section, the mean square displacement (MSD) and diffusion coefficient are calculated to explore how the monomer mobility varies with the salt cation size under different charge fractions. The MSD was computed by averaging over all monomers, as shown in Fig. 8.

As shown in Fig. 8, regardless of the salt cation diameter, the MSD exhibited three distinct power-law scaling regimes with time at different charge fractions. These regimes are delineated by the vertical dashed lines in Fig. 8(a), and follow the relationship MSD $\propto t^{\alpha}$. The exponent α varies with the timescale, reflecting distinct diffusion behaviors. Specifically,

https://doi.org/10.1007/s10118-026-3776-5

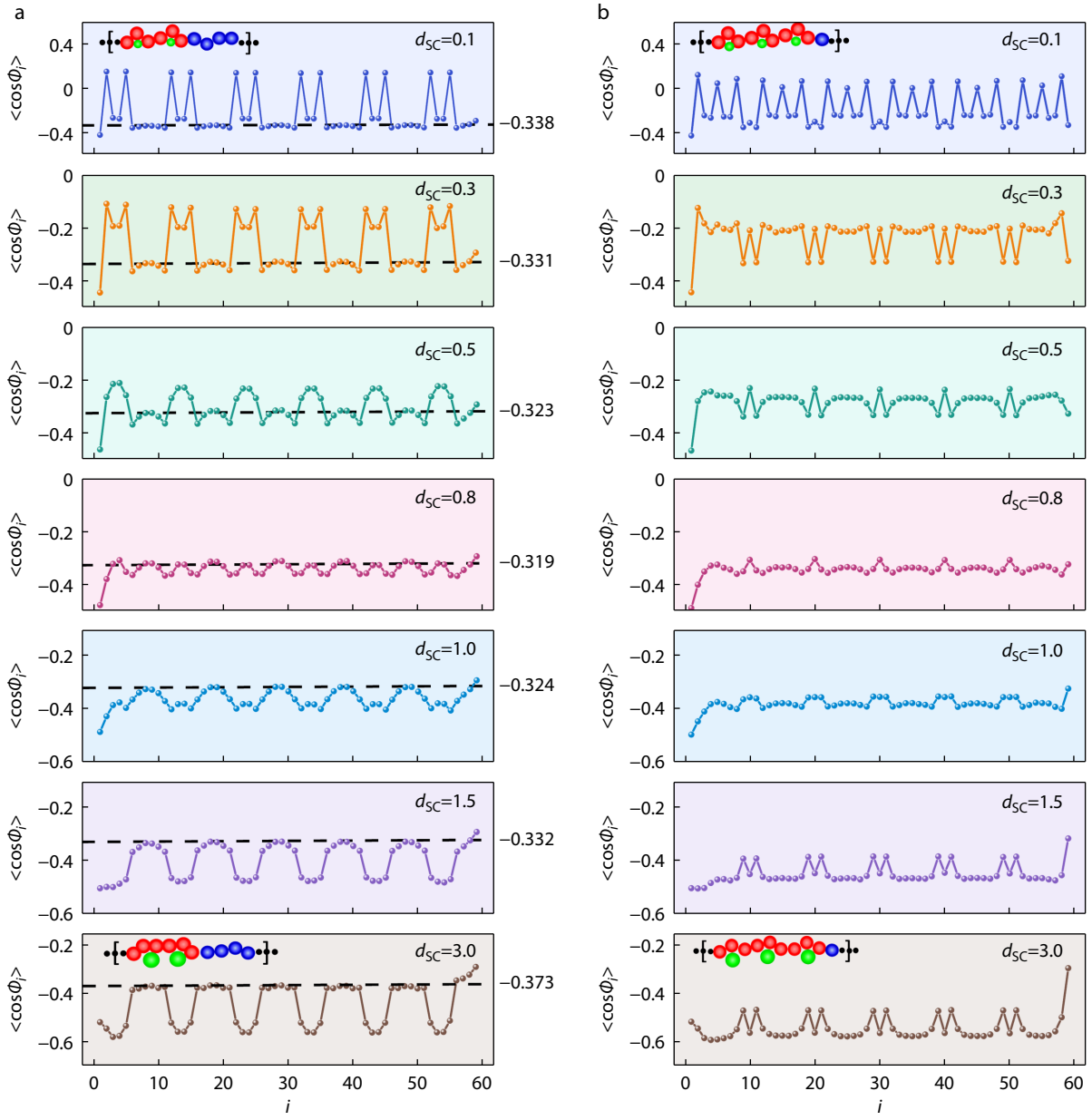

Fig. 7 $\langle \cos\Phi_i \rangle$ of adjacent monomer bond angles as a function of the bond sequence i under varying fractions of charged monomers along the chain. (a) f=0.6 (b) f=0.9 The inset depicts the chain configuration under the respective conditions. The dashed line in the left panels represents the cosine values of the bond angles between the adjacent neutral monomers.

over short time intervals, α=1 indicated a normal diffusion regime. At intermediate timescales, a sub-diffusion regime is observed, characterized by a power-law exponent satisfying $0<\alpha<1$. Over long timescales, α approaches 0, indicating a non-diffusive regime where the MSD remains nearly constant owing to the confinement imposed by the substrate-grafted PE brushes.

In the long-term non-diffusive regime, the MSD curves exhibit distinct responses to increasing salt cation diameter, depending on the charge fraction. Specifically, at relatively low charge fractions, as shown in Figs. 8(a) and 8(b), the MSD curves exhibit minimal differences in their plateau heights, suggesting that the salt cation diameter has a negligible effect on the MSD response. In contrast, when the charge fraction increased to f≥0.5, as illustrated in Figs. 8(c) and 8(d), the MSD curves diverged significantly, and this divergence became more pronounced with increasing charge fraction. This indicates that the influence of the salt cation diameter on the MSD response of the monomers is substantially pronounced at higher charge fractions.

The monomer diffusion coefficient D was obtained by fitting the mean square displacement (MSD) in the early time linear regime using the following relation:

$$\mathrm{MSD}(t) = 2dDt \tag{8}$$

where d denotes the spatial dimension. Because the MSD was computed in three dimensions, we set d=3. Fig. 9 shows the

https://doi.org/10.1007/s10118-026-3776-5

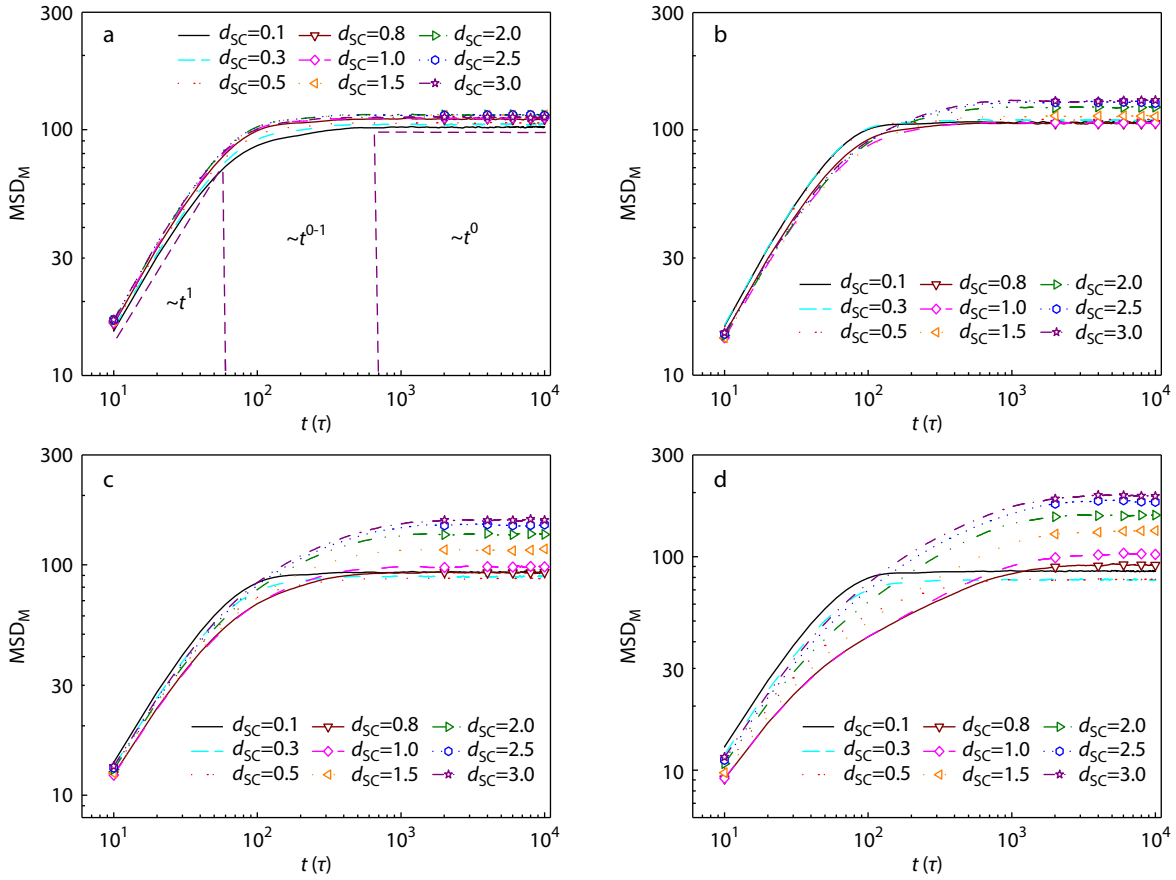

Fig. 8 The mean square distance of monomers at different chain charge fraction with different cation diameters. (a) f=0.1, (b) f=0.3, (c) f=0.5, (d) f=0.8.

monomer diffusion coefficient as a function of the salt cation diameter.

As shown in Fig. 9, the diffusion coefficient exhibits a distinct dependence on the salt cation size depending on the charge fraction. Specifically, at f=0.1, the diffusion coefficient increased monotonically with increasing d_{SC}. The reason for this behavior is that at low charge fractions, increasing the cation diameter weakens the electrostatic attractions between monomers and salt cations, leading to enhanced local mobility of monomers, thus facilitating the diffusion of monomers. When f≥0.3, all diffusion coefficient curves displayed a non-monotonic trend, first decreasing and then increasing with d_{SC}. The initial decrease is attributed to the enhanced electrostatic bridging effect with increasing cation size, which restricts the monomer mobility and reduces the diffusion coefficient. Upon further increasing the cation diameter, the electrostatic attraction weakened, allowing the PE brushes to expand more substantially. This expansion increases the local accessible volume for the monomers, thereby increasing the diffusion coefficient. Moreover, as the charge fraction increased, the bridging effect of salt cations became more pronounced, leading to greater brush heterogeneity and an overall decrease in the diffusion coefficient curve. Notably, the diffusion coefficient reached its minimum at a salt cation diameter of approximately d_{SC}=1.0.

It should be noted that the ionic strength I can affect the conformation of PE brushes.[35,36] Under the simulation conditions, $I \propto f$. The salt ionic strength is not independently controlled, but varies concomitantly with f. An increase in the charge fraction leads to a higher ionic strength of the triva-

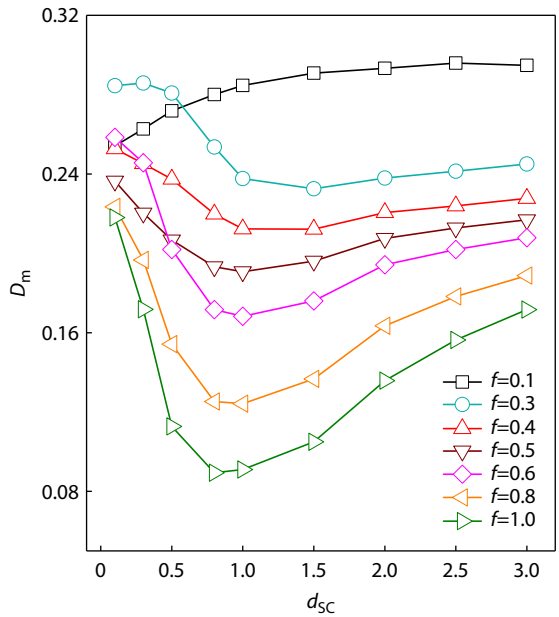

Fig. 9 Diffusion coefficient of monomers as a function of salt cation diameter for different charge fractions.

https://doi.org/10.1007/s10118-026-3776-5

lent salt ions, which amplifies the electrostatic interactions, bridging effect, and excluded volume effect of the salt ions. Competition among these effects consequently alters the brush structure, brush height, and diffusion coefficient. Therefore, the observed trends with respect to f reflect the influence of the charge fraction and corresponding ionic strength.

To provide more direct evidence for the bridging effects discussed above, we followed the approach of van der Vegt *et al.*[34] and analyzed the coordination statistics and bridge lifetimes of trivalent cations. The fractions ψ of the free, mono-coordinated, di-coordinated (inter-chain), and tri-coordinated (inter-chain) cations, as well as the bridge lifetimes obtained from the autocorrelation functions of the salt-bridge networks, were calculated. The results are summarized in Fig. 10 for two representative charge fractions, f=0.3 and f=0.6.

As shown in Figs. 10(a) and 10(b), the fraction of free cations increases monotonically with d_{SC}, which can be rationalized by the weakening of the Coulomb attraction between the larger cations and charged monomers. At f=0.3, as shown in Fig. 10(a), the fractions of di- and tri-coordinated cations first increased and then decreased slightly with d_{SC}. This initial increase indicates that larger cations can more readily contact multiple charged monomers, thereby enhancing the bridging effect. With a further increase in the cation

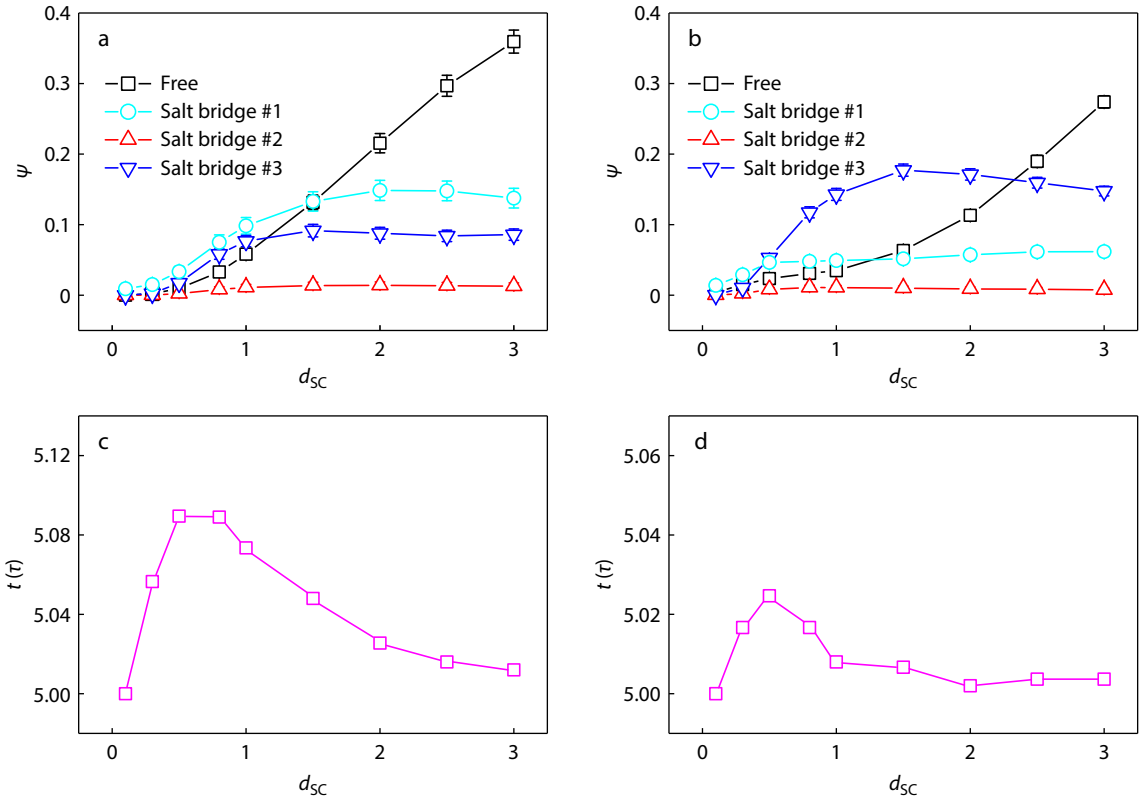

Fig. 10 The fractions ψ of non-coordinated cations, mono-, di- and tri-coordinated salt bridges as a function of d_{SC} at charge fraction (a) f=0.3 and (b) f=0.6. The bridging lifetime as a function of d_{SC} at charge fraction (c) f=0.3 and (d) f=0.6.

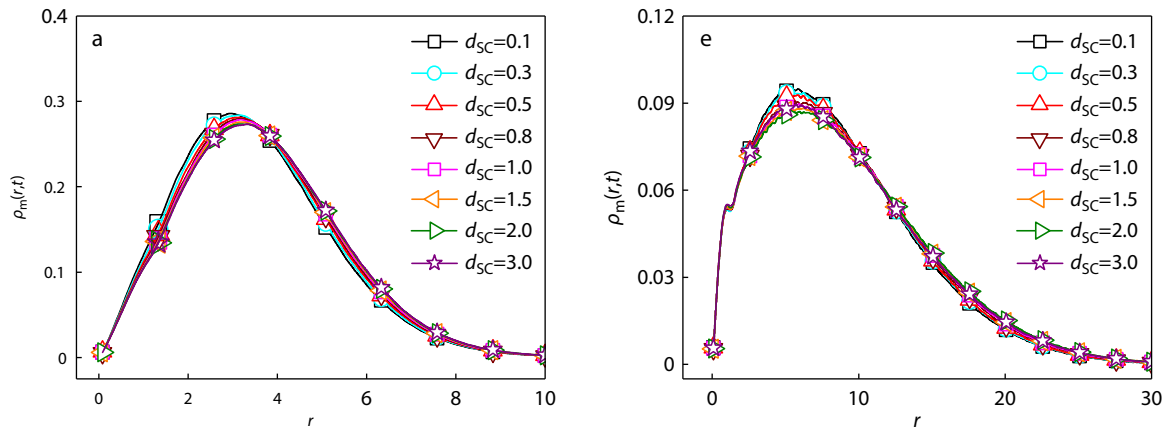

https://doi.org/10.1007/s10118-026-3776-5

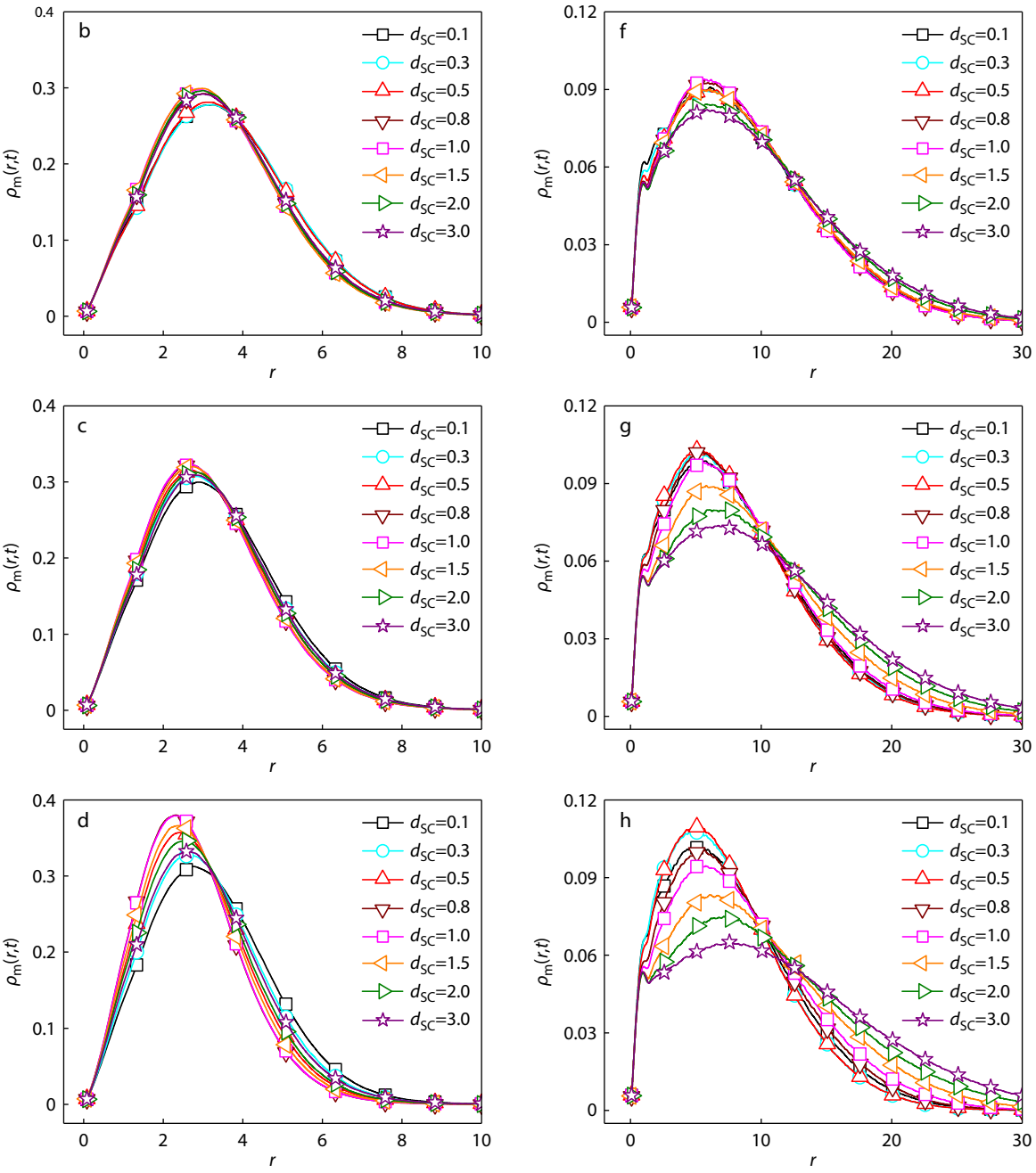

Fig. 11 Probability density function $\rho_m(r,t)$ of monomers for short time interval of 2×10^3 time steps (left panels) and long time interval of 3.2×10^6 time steps (right panels) for (a, e) f=0.1, (b, f) f=0.3, (c, g) f=0.5, (d, h) f=0.8.

size, the electrostatic attraction weakened, leading to a modest reduction in the mono-, di-, and tri-coordinated fractions. At a high charge fraction f=0.6, plotted in Fig. 10(b), tri-coordinated cations dominate, and their fraction also exhibits a non-monotonic dependence on d_{SC}.

From Figs. 10(c) and 10(d), at both charge fractions, the bridge lifetimes first increased and then decreased with increasing d_{SC}. This non-monotonic trend demonstrates that as the cation size increases, the bridging becomes more effective and the complexes persist longer. When the cation becomes too large, the weakened Coulomb attraction reduces the stability of the cation-monomer complexes, shortening their bridge lifetimes.

Time-dependent Probability Density Function

To study the dynamic properties of monomers more carefully, we further calculate the probability density function $\rho_m(r, t)$ of monomers, which captures the probability of a monomer's displacement within the range $[r, r + dr]$ over a given time interval t. Fig. 11 presents $\rho_m(r,t)$ for both short (2×10^3 time steps) and long (3.2×10^6 time steps) time intervals.

As depicted in Figs. 11(a) and 11(e), when the charge fraction is extremely low (f=0.1), $\rho_m(r,t)$ shows minimal sensitivity to the salt cation size over both short and long time intervals.

https://doi.org/10.1007/s10118-026-3776-5

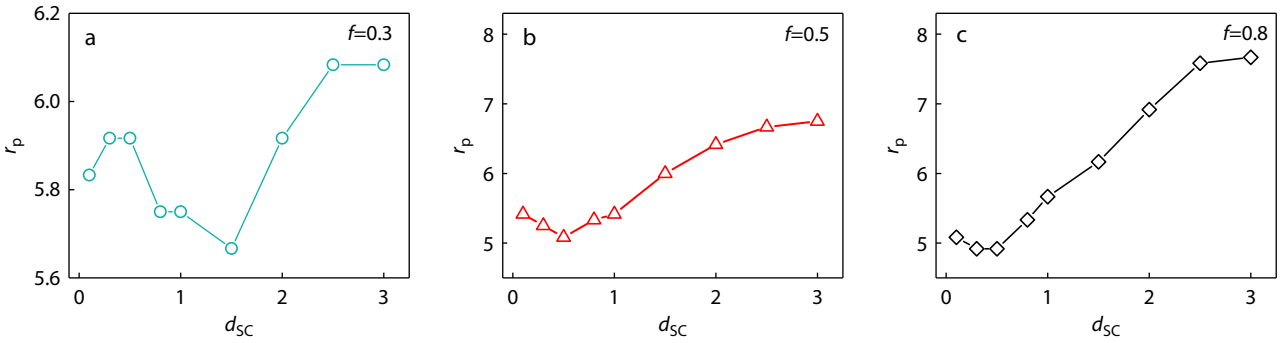

Fig. 12 Peak positions plot of the probability density function $\rho_m(r,t)$ for monomers under long time interval. (a) f=0.3, (b) f=0.5, (c) f=0.8.

As the charge fraction increased, as illustrated in Figs. 11(b) and 11(f), $\rho_m(r,t)$ began to show a dependence on the cation diameter over long time intervals. This dependence becomes increasingly pronounced at higher charge fractions. When the charged fraction reached f=0.8, as shown in Figs. 11(d) and 11(h), $\rho_m(r,t)$ demonstrated clear cation specificity over both short and long time intervals, with the effect being more significant at longer times. Moreover, when the salt cation diameter exceeded 0.5, the peak intensity gradually decreased with increasing cation diameter, whereas the overall curve broadened, indicating an increasingly diverse motion of the monomers. The variations in the peak position r_p of the $\rho_m(r,t)$ curve over a long time interval are further analyzed in Fig. 12.

As shown in Fig. 12, the response of r_p to the salt cation diameter exhibits distinct profiles with increasing charge fraction. Specifically, as shown in Fig. 12(a), at a charge fraction of f=0.3, r_p initially increases, then decreases, and subsequently increases again as the cation diameter increases. The reason for this behavior is that electrostatic attraction between the monomers and salt cations is dominant at small cation diameters. As the cation diameter increased, this electrostatic attraction weakened, allowing monomers to move over a broader range. With a further increase in the cation diameter, the electrostatic bridging effect of the salt cations becomes dominant, weakening the monomer mobility. Upon further increasing the cation diameter, the volume effect gradually prevailed, causing the brushes to become increasingly loose. Concurrently, the electrostatic interactions between the monomers and salt cations diminish, leading to re-expansion of the monomer motion range. At charge fractions f≥0.5, the competing effects of bridging and volume effects cause r_p to first decrease and then increase with increasing cation diameter, as shown in Figs. 12(b) and 12(c).

CONCLUSIONS

Using coarse-grained MD simulations, we systematically investigated the coupled effects of trivalent cation size and charge fraction on the structural and dynamical properties of planar PE brushes. Our results reveal that the interplay between cation size and charge fraction can induce interesting surface morphologies, such as laterally homogeneous collapsed structures, pinned micelles, and swollen layers. When the cation size was small, the brushes exhibited a homogeneous structure, with only a weak dependence on the charge fraction. For intermediate cation sizes, inter-chain bridging became increasingly pronounced as the charge fraction increased, leading to marked lateral heterogeneity and the formation of multi-chain domains, which were most prominent when the cation dimensions were commensurate with the monomer size. Upon further increase in the cation size, the brushes evolved into a homogeneous layered morphology at high charge fractions. The brush height displayed three distinct regimes as a function of the charge fraction: at extremely small cation sizes, a weakly oscillatory trend; at intermediate cation sizes, a monotonic decrease; and at sufficiently large cation sizes, a monotonic increase. Furthermore, through the analysis of bond angle distributions, the single-chain conformation was found to exhibit markedly distinct responses depending on the specific combination of the charge fraction and cation size.

Dynamically, the diffusion behavior of PE monomers is also strongly influenced by the coupling of the charge fraction and cation size. At low charge fractions, monomer diffusion increases monotonically with cation size, as the weakening of electrostatic attraction enhances the local mobility. At high charge fractions, the diffusion coefficient exhibited a non-monotonic dependence, first decreasing and then increasing with cation size, reaching a minimum at a cation size of approximately 1.0. This minimum corresponds to the strongest bridging effect, which restricts the monomer motion. Correspondingly, the monomer displacement range over long time intervals exhibits complex, non-monotonic behavior: it increases, then decreases, and finally increases again with increasing cation diameter, reflecting competition among electrostatic attraction, bridging, and volume effects. In contrast, at high charge fractions, only two regimes are observed: initial restriction followed by subsequent expansion, indicating that the bridging effect dominates at smaller cation sizes, while volume effects dominate at larger sizes.

In summary, the synergistic interplay between the charge fraction and trivalent cation size governs the PE brush properties through a balance of electrostatic interactions, cation-induced bridging, and excluded volume repulsion. At low charge fractions, sparsely charged monomers suppress the bridging. As the charge fraction increased, bridging and electrostatic screening dominated, especially when the cation size matched the monomer dimension, leading to lateral heterogeneity, reduced brush height, and restricted diffusion. Further increasing the cation size shifted the balance to exclude volume dominance, promoting swelling and enhanced diffusion. Thus, the charge fraction controls the bridging propensity *via* charged monomer density, while cation size determines whether electrostatic interactions, bridging, or volume exclusion prevail, collectively yielding diverse re-

https://doi.org/10.1007/s10118-026-3776-5

sponses in brush height and dynamics, providing guidance for designing stimulus-responsive PE brushes.

Conflict of Interests

The authors declare no interest conflict.

Data Availability Statement

The data that support the findings of this study are available from the corresponding author upon reasonable request.

ACKNOWLEDGMENTS

This work was financially supported by the Fundamental Research Funds for Central Universities (No. 3122020080) and the Graduate Research Project of Civil Aviation University of China (No. 2024YJSKC06005).

REFERENCES

1 Yang, Q.; Li, L.; Zhao, F.; Han, H.; Wang, W.; Tian, Y.; Wang, Y.; Ye, Z.; Guo, X. Hollow silica–polyelectrolyte composite nanoparticles for controlled drug delivery. *J. Mater. Sci.* **2019**, *54*, 2552–2565.
2 Yu, Y.; de la Cruz, R. A. L.; Kieviet, B. D.; Gojzewski, H.; Pons, A.; Vancso, G. J.; de Beer, S. Pick up, move and release of nanoparticles utilizing co-non-solvency of PNIPAM brushes. *Nanoscale* **2017**, *9*, 1670–1675.
3 Yu, Y.; Kieviet, B. D.; Kutnyanszky, E.; Vancso, G. J.; de Beer, S. Cosolvency-induced switching of the adhesion between poly (methyl methacrylate) brushes. *ACS Macro Lett.* **2015**, *4*, 75–79.
4 Psarra, E.; König, U.; Ueda, Y.; Bellmann, C.; Janke, A.; Bittrich, E.; Eichhorn, K.-J.; Uhlmann, P. Nanostructured biointerfaces: nanoarchitectonics of thermoresponsive polymer brushes impact protein adsorption and cell adhesion. *ACS Appl. Mater. Interfaces* **2015**, *7*, 12516–12529.
5 Sachar, H. S.; Sivasankar, V. S.; Das, S. Electrokinetic energy conversion in nanochannels grafted with pH-responsive polyelectrolyte brushes modelled using augmented strong stretching theory. *Soft Matter* **2019**, *15*, 5973–5986.
6 Zhang, T.; Lu, Q.; Zhang, X.; Liu, S.; Ye, Q.; Zhou, F. Fabrication of polyelectrolyte brush-functionalized two-dimensional covalent organic frameworks as additives for aqueous lubricants. *Tribol. Int.* **2022**, *174*, 107737.
7 Zhulina, E. B.; Rubinstein, M. Lubrication by polyelectrolyte brushes. *Macromolecules* **2014**, *47*, 5825–5838.
8 Kobayashi, M.; Terada, M.; Takahara, A. Polyelectrolyte brushes: a novel stable lubrication system in aqueous conditions. *Faraday Discuss.* **2012**, *156*, 403.
9 Li, B.; Yu, B.; Wang, X.-L.; Guo, F.; Zhou, F. Correlation between conformation change of polyelectrolyte brushes and lubrication. *Chinese J. Polym. Sci.* **2015**, *33*, 163–172.
10 Liu, G.; Liu, Z.; Li, N.; Wang, X.; Zhou, F.; Liu, W. Hairy polyelectrolyte brushes-grafted thermosensitive microgels as artificial synovial fluid for simultaneous biomimetic lubrication and arthritis treatment. *ACS Appl. Mater. Interfaces* **2014**, *6*, 20452–20463.
11 Smook, L. A.; Dahlin, A.; Schroën, K.; de Beer, S. Responsive polyelectrolyte brushes in applications: functions, stimuli, and design considerations. *Adv. Mater.* **2025**, *37*, e09580.
12 Sachar, H. S.; Pial, T. H.; Chava, B. S.; Das, S. All-atom molecular dynamics simulations of weak polyionic brushes: influence of charge density on the properties of polyelectrolyte chains, brush-supported counterions, and water molecules. *Soft Matter* **2020**, *16*, 7808–7822.
13 Mahalik, J. P.; Yang, Y.; Deodhar, C.; Ankner, J. F.; Lokitz, B. S.; Kilbey, S. M. II, Sumpter, B. G.; Kumar, R. Monomer volume fraction profiles in pH responsive planar polyelectrolyte brushes. *J. Polym. Sci., Part B: Polym. Phys.* **2016**, *54*, 956–964.
14 Pial, T. H.; Sachar, H. S.; Das, S. Quantification of mono- and multivalent counterion-mediated bridging in polyelectrolyte brushes. *Macromolecules* **2021**, *54*, 4154–4163.
15 Ishraaq, R.; Das, S. All-atom molecular dynamics simulations of cationic polyelectrolyte brushes in the presence of halide counterions. *Macromolecules* **2024**, *57*, 3037–3046.
16 Xu, X.; Mastropietro, D.; Ruths, M.; Tirrell, M.; Yu, J. Ion-specific

Graphical Abstract

Surface Morphologies and Dynamic Properties of Polyelectrolyte Brushes Induced by Charge Fraction and Cationic Size

Hong-Yan Zhang, Qing-Hai Hao, Ming-Lu Chao, and Hong-Ge Tan

Civil Aviation University of China

Varying chain charge fraction and salt cation size lead to rich responsive characteristics in the structure and height of polyelectrolyte brushes, which offers novel insights into developing stimuli-responsive polyelectrolyte brushes.

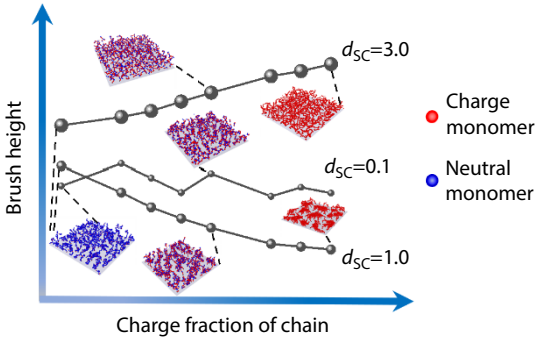

Chinese J. Polym. Sci. 2026 *https://doi.org/10.1007/s10118-026-3776-5*

effects of divalent ions on the structure of polyelectrolyte brushes. *Langmuir* **2019**, *35*, 15564−15572.
17 Smook, L. A.; de Beer, S. Molecular design strategies to enhance the electroresponse of polyelectrolyte brushes: effects of charge fraction and chain length dispersity. *Macromolecules* **2025**, *58*, 1185−1195.
18 Yu, J.; Jackson, N. E.; Xu, X.; Brettmann, B. K.; Ruths, M.; de Pablo, J. J.; Tirrell, M. Multivalent ions induce lateral structural inhomogeneities in polyelectrolyte brushes. *Sci. Adv.* **2017**, *3*, eaao1497.
19 Gioldasis, C.; Gergidis, L. N.; Vlahos, C. Complexation of a polyelectrolyte brush with oppositely charged AB diblock copolymers: the zipper brushes. *Macromol. Theory Simul.* **2022**, *31*, 2200011.
20 Smook, L. A.; de Beer, S. The effect of salt and monomer distribution on the electroresponse of partially charged polyelectrolyte brushes. *J. Polym. Sci.* **2025**, *63*, 3446−3455.
21 Prusty, D.; Gallegos, A.; Wu, J. Modeling ionic and sequence effects on the swelling behavior of polyampholyte brushes. *Macromolecules* **2024**, *57*, 6666−6680.
22 Duan, C.; Agrawal, N. R.; Wang, R. Electrostatic correlation augmented self-consistent field theory and its application to polyelectrolyte brushes. *Phys. Rev. Lett.* **2025**, *134*, 048101.
23 Yu, J.; Mao, J.; Yuan, G.; Satija, S.; Jiang, Z.; Chen, W.; Tirrell, M. Structure of polyelectrolyte brushes in the presence of multivalent counterions. *Macromolecules* **2016**, *49*, 5609−5617.
24 Li, M.; Zhuang, B.; Yu, J. Effects of ion valency on polyelectrolyte brushes: a unified theory. *Macromolecules* **2022**, *55*, 10450−10456.
25 Jackson, N. E.; Brettmann, B. K.; Vishwanath, V.; Tirrell, M.; de Pablo, J. J. Comparing solvophobic and multivalent induced collapse in polyelectrolyte brushes. *ACS Macro Lett.* **2017**, *6*, 155−160.
26 Kim, Y. C.; Hoang, S.; Winey, K. I.; Composto, R. J. Size-dependent electrostatic adsorption of polymer-grafted gold nanoparticles on polyelectrolyte brushes. *ACS Appl. Mater. Interfaces* **2024**, *16*, 61083−61095.
27 Philippova, O. E.; Rumyantsev, A. M.; Kramarenko, E. Y.; Khokhlov, A. R. New type of swelling behavior upon gel ionization: theory vs experiment. *Macromolecules* **2013**, *46*, 9359−9367.
28 Tagliabue, A.; Mella, M. The role of counterion size in defining star-shaped polyelectrolytes thermodynamics, conformations, and ion dynamics. *J. Polym. Sci.* **2025**, *63*, 3005−3022.
29 Kremer, K.; Grest, G. S. Dynamics of entangled linear polymer melts: A molecular-dynamics simulation. *J. Chem. Phys.* **1990**, *92*, 5057−5086.
30 Murat, M.; Grest, G. S. Molecular dynamics study of dendrimer molecules in solvents of varying quality. *Macromolecules* **1996**, *29*, 1278−1285.
31 Plimpton, S. Fast parallel algorithms for short-range molecular dynamics. *J. Comput. Phys.* **1995**, *117*, 1−19.
32 Carrillo, J. Y.; Dobrynin, A. V. Polyelectrolytes in salt solutions: molecular dynamics simulations. *Macromolecules* **2011**, *44*, 5798−5816.
33 Carrillo, J. Y.; Brown, W. M.; Dobrynin, A. V. Explicit solvent simulations of friction between brush layers of charged and neutral bottle-brush macromolecules. *Macromolecules* **2012**, *45*, 8880−8891.
34 Rodríguez-Ropero, F.; van der Vegt, N. F. A. Ionic specific effects on the structure, mechanics and interfacial softness of a polyelectrolyte brush. *Faraday Discuss.* **2013**, *160*, 297−309.
35 Safi Samghabadi, F.; Ramezani Bajgiran, S.; Villegas Orellana, M.; Conrad, J. C.; Marciel, A. B. Charge state of weak polyelectrolyte brushes determines salt-dependent swelling and hysteretic behavior. *ACS Macro Lett.* **2024**, *13*, 1570−1576.
36 Robertson, H.; Elliott, G. R.; Nelson, A. R. J.; Le Brun, A. P.; Webber, G. B.; Prescott, S. W.; Craig, V. S. J.; Wanless, E. J.; Willott, J. D. Underscreening in concentrated electrolytes: re-entrant swelling in polyelectrolyte brushes. *Phys. Chem. Chem. Phys.* **2023**, *25*, 24770−24782.

https://doi.org/10.1007/s10118-026-3776-5